Science of the Total Environment 690 (2019) 932–943

Contents lists available at ScienceDirect

Science of the Total Environment

journal homepage: www.elsevier.com/locate/scitotenv

Impacts of meteorological factors and land use pattern on hydrological elements in a semi-arid basin

Ting Huang [a], Deyong Yu [a,*], Qian Cao [b], Jianmin Qiao [c]

[a] Center for Human-Environment System Sustainability (CHESS), State Key Laboratory of Earth Surface Processes and Resource Ecology (ESPRE), Faculty of Geographical Science, Beijing Normal University, Beijing 100875, China
[b] Institute of Ecology and Biodiversity, School of Life Sciences, Shandong University, Qingdao 266237, China
[c] School of Geography and Environment, Shandong Normal University, Jinan 250014, China

HIGHLIGHTS

- LAI improved the accuracy of simulating spatial hydrological elements.
- Influential factors on hydrological elements varied according to the land use type.
- Landscape management can promote optional utilization of water resources.

GRAPHICAL ABSTRACT

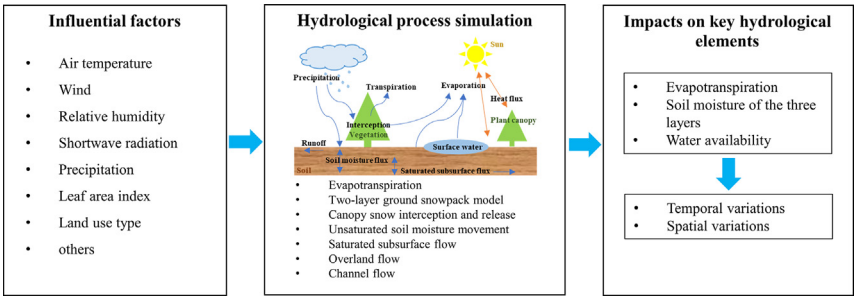

ARTICLE INFO

Article history:
Received 28 March 2019
Received in revised form 27 June 2019
Accepted 5 July 2019
Available online 05 July 2019

Editor: Ouyang Wei

Keywords:
Hydrological modeling
LAI
Landscape heterogeneity
Water resources management

ABSTRACT

The allocation of water resources to meet both human wellbeing and environmental requirements is a critical challenge in a semi-arid landscape. Hydrological models are widely used to understand the influence mechanism of hydrological elements, which is helpful for optimizing water resources management. However, the spatial heterogeneity of hydrological dynamics has been largely omitted in prior studies, partly because it's difficult to correctly simulate the spatial distributions of hydrological elements due to roughly representing the surface biophysical parameters in the hydrological model. In this study, the Distributed Hydrological Soil Vegetation Model (DHSVM) was incorporated with the high-resolution remotely sensed leaf area index (LAI) data in a semi-arid basin, located in the upstream of the Xar Moron River Basin, to explore the impacts of meteorological factors (i.e., air temperature, wind speed, relative humidity, shortwave radiation, and precipitation) and LAI on hydrological processes of forests, grasslands, and farmlands. Our results show that the spatial distribution of LAI slightly improves the accuracy of streamflow simulations and significantly promotes the model performance of spatial hydrological element simulations. For the area in study, precipitation, LAI, and relative humidity are the three major influential factors in the forest hydrological dynamics. The hydrological elements of grasslands and farmlands are mainly affected by shortwave radiation, relative humidity, air temperature, and LAI. Compared with grasslands and farmlands, LAI has greater negative influence on forest water availability. To mitigate the negative effects of drying and warming climate and promote ecosystems sustainability, the forest area should be converted into grassland while the native grassland should be maintained for soil water conservation.

* Corresponding author at: No.19 XinJieKouWai Street, Beijing 100875, China.
E-mail address: ydy@bnu.edu.cn (D. Yu).

https://doi.org/10.1016/j.scitotenv.2019.07.068
0048-9697/

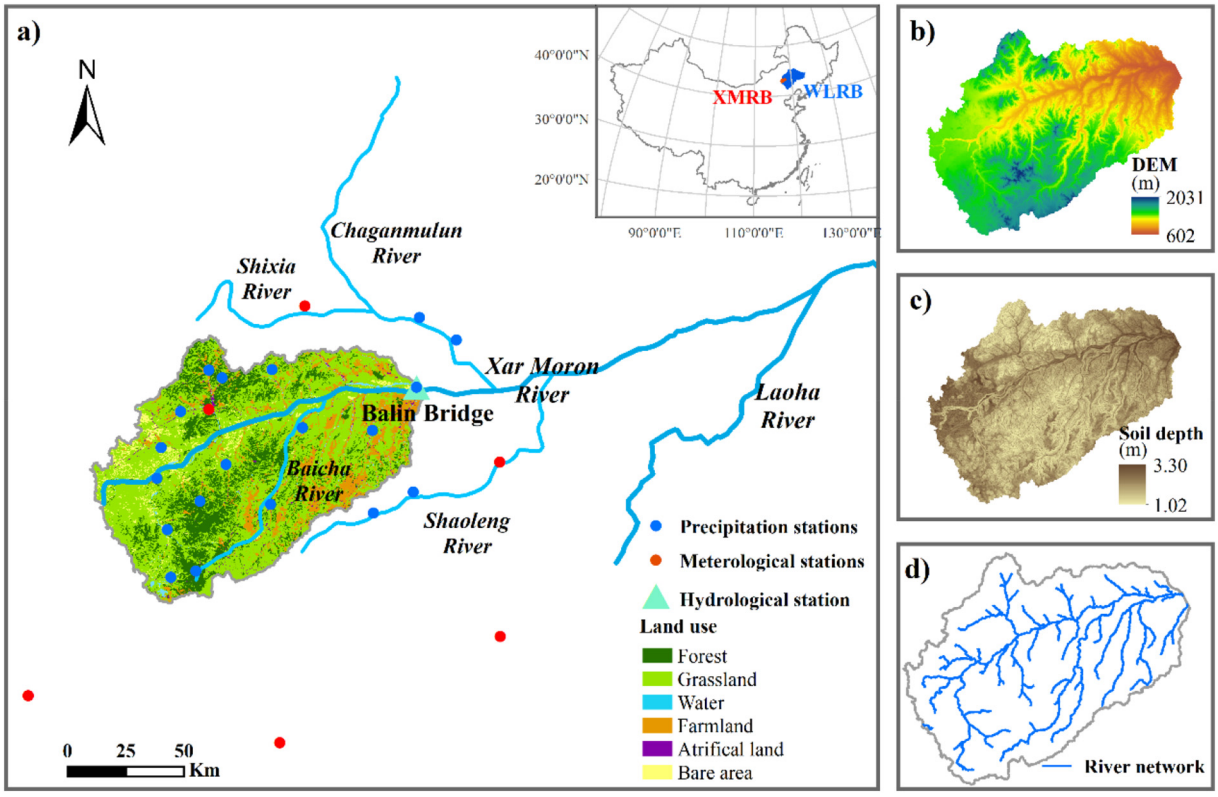

Fig. 1. Description of the study area, including a) the location of the study area, the land use types during 2011 to 2013, b) the DEM, and c) the soil depth and d) river network derived from the DEM.

1. Introduction

Water is not just an essential natural resource for human production and life but also plays an important role in maintaining ecosystem functions. Proper distribution of water resources is significant for socioeconomic development and ecosystem sustainability. Runoff is closely related to water yield while soil water plays an important role in water retention, soil conservation, vegetation growth and recovery (Ma et al., 2006). Evapotranspiration is a key component of the hydrological cycle, which greatly impacts water resource distribution in the soil-plant-atmosphere continuum. In the arid and semi-arid regions, water resource loss is dominated by evapotranspiration (Huxman et al., 2005; Sun et al., 2011). Prior studies indicate that hydrological elements can be highly sensitive to regional meteorological conditions (Schnorbus et al., 2014; Stagl et al., 2014; Liu et al., 2015) and land use patterns (Vanshaar et al., 2002; Fu et al., 2005; Thanapakpawin et al., 2007). Variations of the meteorological factors, such as precipitation and temperature, can lead to direct or indirect changes in runoff (van Dam, 2003). Different land use patterns,

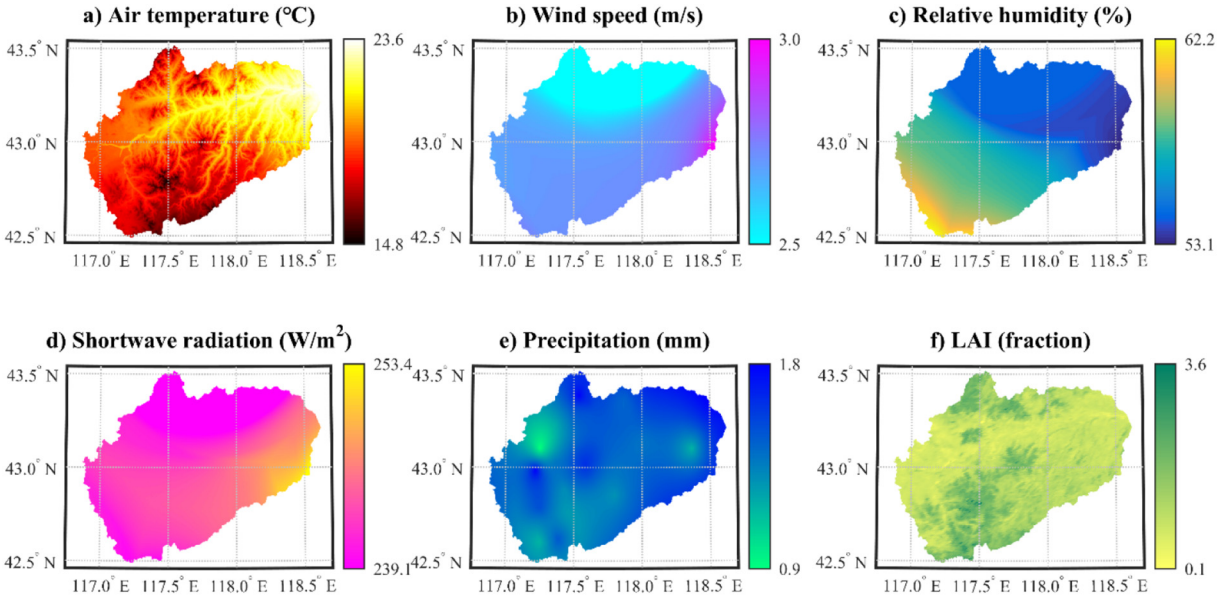

Fig. 2. Daily mean values of the six influential factors during the growing season from 2011 to 2013.

Table 1
Soil parameters of the four main soil types used in the DHSVM.

Soil parameters	Loam	Sand	Silt loam	Sandy loam
Lateral saturated hydraulic conductivity (m/s) [d]	9.5E-06	3.4E-05	9.0E-06	1.1E-05
Exponential decrease [e]	0.1	0.1	1	1
Depth threshold [a]	0.5	0.5	0.5	0.5
Maximum infiltration (m/s) [b]	5.0E-04	5.0E-04	5.0E-04	1.0E-03
Number of soil Layers [a]	3	3	3	3
Porosity (fraction) (fraction) [d]	0.444	0.46	0.461	0.437
Pore size distribution (fraction) [c]	0.252	0.694	0.234	0.378
Bubbling pressure (m) [c]	0.112	0.073	0.208	0.147
Field capacity (fraction) [d]	0.261	0.077	0.299	0.172
Wilting point (fraction) [d]	0.123	0.032	0.107	0.076
Bulk density (kg/m^3) [d]	1471.4	1429.9	1426.2	1491.5
Vertical conductivity (m/s) [b]	9.5E-06	3.4E-05	9.0E-06	1.1E-05
Thermal conductivity (W/m K) [b]	7.1	7.1	7.1	7.1
Thermal capacity (J/m^3 K) [b]	1.4E + 06	1.4E + 06	1.4E + 06	1.4E + 06

[a] Model defaults.
[b] Campbell and Norman (1979).
[c] Stieglitz et al. (1997).
[d] Saxton (1989).
[e] Lan et al. (2011b).

Table 2
Vegetation parameters of the three main land use types used in the DHSVM.

Vegetation parameters	Woodland		Grassland	Cropland
	Overstory	Understory		
Fractional coverage (fraction) [b]	0.85	–	–	–
Trunk space (fraction) [b]	0.45	–	–	–
Aerodynamic attenuation [f]	1	–	–	–
Radiation attenuation [g]	0.2	–	–	–
Max snow int capacity (fraction) [c]	0.06	–	–	–
Snow interception eff (fraction) [a]	0.8	–	–	–
Mass release drip ratio (fraction) [a]	0.2	–	–	–
Height (m) [h]	12	0.4	0.5	0.6
Maximum resistance (s/m) [c]	3000	1500	1500	1500
Minimum resistance (s/m) [h]	110	60	60	60
Moisture threshold (fraction) [d]	0.2	0.1	0.1	0.1
Vapor pressure deficit (Pa) [h]	4000	4000	4000	4000
Rpc [e]	0.2	0.1	0.1	0.1
Number of root zones [a]	3	3	3	3
Root zone depths (for each zone, m) [d]	0.2		0.2	0.2
	0.4		0.4	0.4
	0.4		0.4	0.4
Root fraction (for each zone, fraction) [d]	0.2	0.6	0.6	0.6
	0.2	0.4	0.4	0.4
	0.6	0	0	0

[a] Model defaults.
[b] Field observation.
[c] Breuer et al. (2003).
[d] Meyer et al. (1997).
[e] Sellers et al. (1994).
[f] Goudriaan (1977).
[g] Nijssen and Lettenmaier (1999).
[h] Lan et al. (2011b).

Table 3
Comparison on four metrics (i.e., NSE, R^2, RMSE, and PBIAS) for both calibration and verification periods.

	L_Class				L_Pixel			
	NSE	R^2	RMSE	PBIAS (%)	NSE	R^2	RMSE	PBIAS (%)
Calibration	0.51	0.54	11.27	10.4	0.52	0.56	10.65	−0.54
Verification	0.46	0.52	7.12	26.02	0.47	0.54	6.83	9.56

which have specific land surface biophysical features, can result in variation of water and energy allocation processes such as radiation transmission and canopy interception (Eagleson, 2005; Jiao et al., 2017). Therefore, exploring how the meteorological factors and land use pattern impact hydrological elements can enhance our understanding of the hydrological cycle and promote a sustainable management of water resources.

To investigate the impacts of different meteorological factors and land use pattern on complex hydrological processes, hydrological models have been widely used in various watersheds. For example, Zhang et al. (2016) simulated hydrological processes in the Heihe River Basin, northwest China, using the Soil Water Assessment Tool (SWAT; Arnold and Fohrer, 2005) model and found that the expansion of grassland and the decrease of farmland reduced runoff and groundwater discharge while a wetting and warming climate increased them. Alvarenga et al. (2016) simulated hydrological processes under different land use scenarios using the Distributed Hydrology Soil Vegetation Model (DHSVM; Wigmosta et al., 1994) and found that deforestation in the Atlantic Forest, Brazil increased soil moisture and runoff and reduced evapotranspiration and water table depth. Hydrological responses of the Tibetan Plateau under different climate change scenarios were generated based on the simulation results of the Variable Infiltration Capacity (VIC; Haddeland et al., 2006) model and showed that the increasing precipitation can increase mean and extreme streamflow while rising air temperature can decrease snowfall and snow water equivalent (Zhong et al., 2018). These researches mainly focused on the overall hydrological respond to changes in meteorological factors and land use pattern. In contrast, few studies have payed attention to the spatial heterogeneity of hydrological dynamics caused by local specific topography (Fujimoto et al., 2008; Ma et al., 2016) and land surface features (Zhang and Wegehenkel, 2006). It's partly because of the difficulty to correctly simulate the spatial distributions of hydrological factors due to the insufficient representation of surface biophysical parameters (e.g., vegetation fraction, leaf area index, and albedo).

Although various hydrological models have incorporated surface biophysical parameters in different land use types, the importance of the spatiotemporal distribution of these parameters is largely omitted (Gao et al., 2018). Recent work has increasingly recognized this limitation (Donohue et al., 2007; Xu et al., 2014; Yang et al., 2016). Especially, leaf area index (LAI), which is widely used to describe the photosynthetic and transpirational surface of plant canopies (Chen et al., 1997), has been utilized with higher accuracy in some researches. The MODIS-derived dynamic LAI is incorporated into the VIC model to enable an interannually varying seasonal cycle of vegetation, which improves the accuracy of the temporal variabilities of river discharge

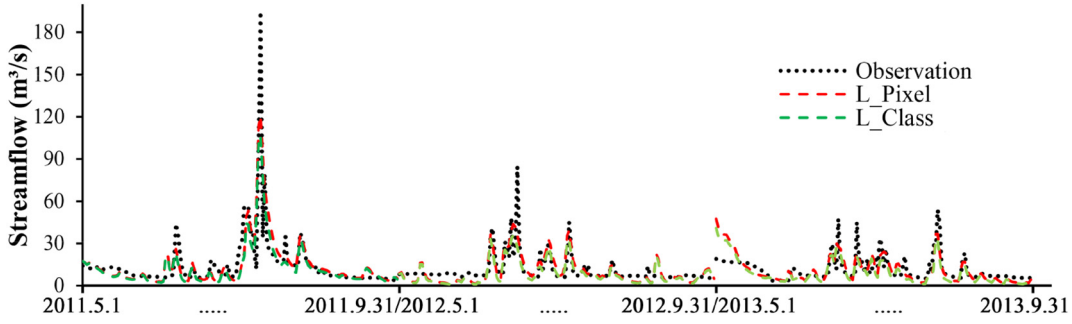

Fig. 3. Observed and simulated daily streamflow (m^3/s) during the growing season from 2011 to 2013.

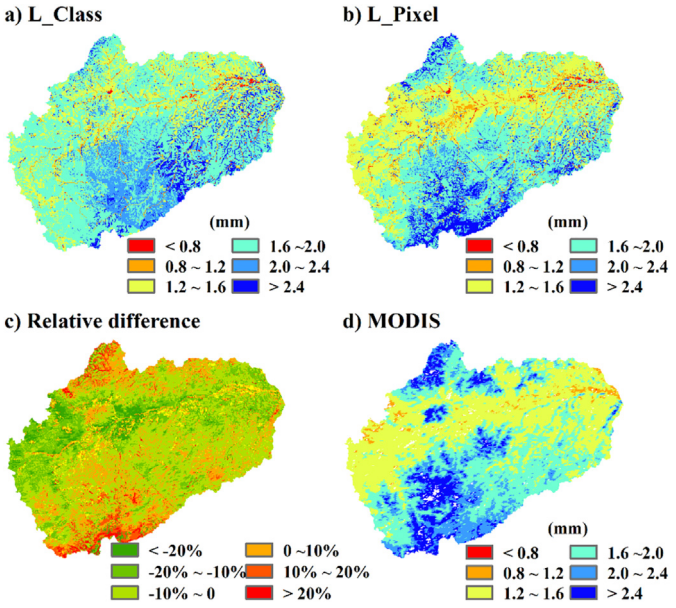

Fig. 4. Simulated daily mean evapotranspiration in a) L_Class and b) L_Pixel, and c) their relative difference (L_Pixel minus L_Class divided by L_Class) as well as d) daily mean MODIS evapotranspiration during the growing season.

(Parr et al., 2015) and soil moisture (Ford and Quiring, 2013). The Weather Research and Forecasting (WRF; Skamarock and Klemp, 2008) model is used to simulate evapotranspiration with different combinations of two land surface models and two LAI datasets (default USGS LAI and high-resolution MODIS LAI), and these four simulations show that the increase in LAI accuracy generally improves the estimation of actual evapotranspiration (Xu et al., 2017). These simulations also indicate that the high complexity surface processes model should be coupled with high accuracy in representations of both LAI and land use types (Cao et al., 2015). In addition, taking both climate- and human-induced LAI (i.e., real value of LAI) change into account can improve the accuracy of hydrological simulation (Jiao et al., 2017). From the above, the spatiotemporal dynamic of LAI should be considered in order to accurately assess hydrological effects of different meteorological factors and land use pattern.

In this study, the DHSVM, a high-complexity hydrological model, was incorporated with the high-resolution remotely sensed LAI to simulate the hydrological processes in a semi-arid basin. The objectives of this paper are to evaluate the potential of remotely sensed LAI data to improve the accuracy of hydrological simulations and to quantify the impacts of meteorological factors (i.e., air temperature, wind speed, relative humidity, shortwave radiation, and precipitation) and LAI on spatial hydrological elements (i.e., evapotranspiration, soil moisture) and water availability (Precipitation minus evapotranspiration) in different land use types during the growing season (from May to September; Zhang et al., 2011) at the pixel scale. This study is expected to accelerate the understanding of influence mechanisms in water resource distribution, and explore an appropriate landscape management scheme for promoting optional water resource utilization in a semi-arid basin.

In the following, the model, experimental design, and datasets are first described in Section 2. The results and discussions are presented in Section 3, including the model evaluation, hydrological dynamics and their influential factors analysis. Furthermore, conclusions are provided in Section 4.

2. Materials and methods

2.1. Study area

The West Liaohe River Basin (WLRB) is located in eastern China, and the Xar Moron River (XMR) is one of the main tributaries of the WLRB (Fig. 1a). In the past 30 years, streamflow of the XMR showed a wavelike decreasing trend, with an annual average runoff of 658 million m^3 (Wu et al., 2014). Our study area is in the upper reaches of the Xar Moron River Basin (XMRB) and has a drainage area of 11, 207 km^2. The Balin Bridge hydrological station (118°37′ E, 43°15′ N) is at the watershed outlet. Natural stream flow in the downstream of XMRB has been greatly disturbed by storage projects and lift irrigation. While this disturbance is relatively small in our study area, especially during the period of 2011—2013 (Hydrological Bureau et al., 2014). The maximum streamflow of the Balin Bridge hydrological station during this period is 192 m^3/s, while in the winter the streamflow is almost zero. The study area ranges in elevation from 602 m to 2031 m (Fig. 1b). Grassland, forest (mainly deciduous broadleaf forest), and farmland are the three major land use types, accounting for 61.6%, 19.8%, and 12.3% of the study area, respectively (Fig. 1a).

The study area is located in a typical temperate semi-arid continental monsoon climate zone. During the growing season (from May to September) from 2011 to 2013, daily mean air temperature increases from the southwest to the northeast, and daily mean air temperatures of forest, grassland, and farmland are 18.5 °C, 19.7 °C and 20.3 °C, respectively (Fig. 2a). Daily mean precipitation of the forest (i.e., 1.51 mm) is slightly larger than that of grassland and farmland (i.e. 1.46 mm) (Fig. 2e), while daily mean LAI of the forest (i.e., 1.61) is significantly larger than that of the other two land use types (i.e., 1.03) (Fig. 2f). Wind speed, relative humidity, and shortwave radiation of different land use types have little difference in both variation trend and magnitude (Fig. S1). During the growing season, basin-averaged wind speed, relative humidity, and shortwave radiation are 2.68 m/s, 56.2%, and 242.87 W/m^2, respectively (Fig. 2 b, c, d). Due to windy and arid climate conditions and extensive human activities, this basin suffered serious vegetation degradation and soil erosion in the past decades.

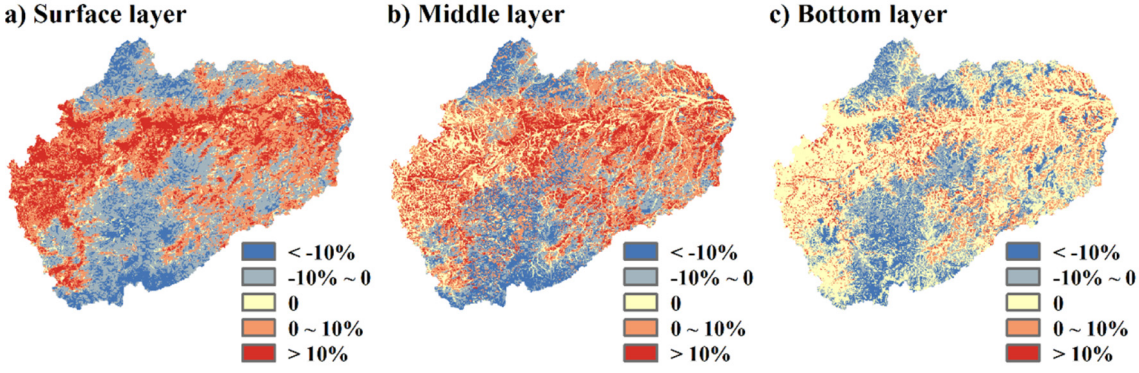

Fig. 5. Relative difference (L_Pixel minus L_Class divided by L_Class) of simulated daily mean soil moisture of three layers in L_Class and L_Pixel.

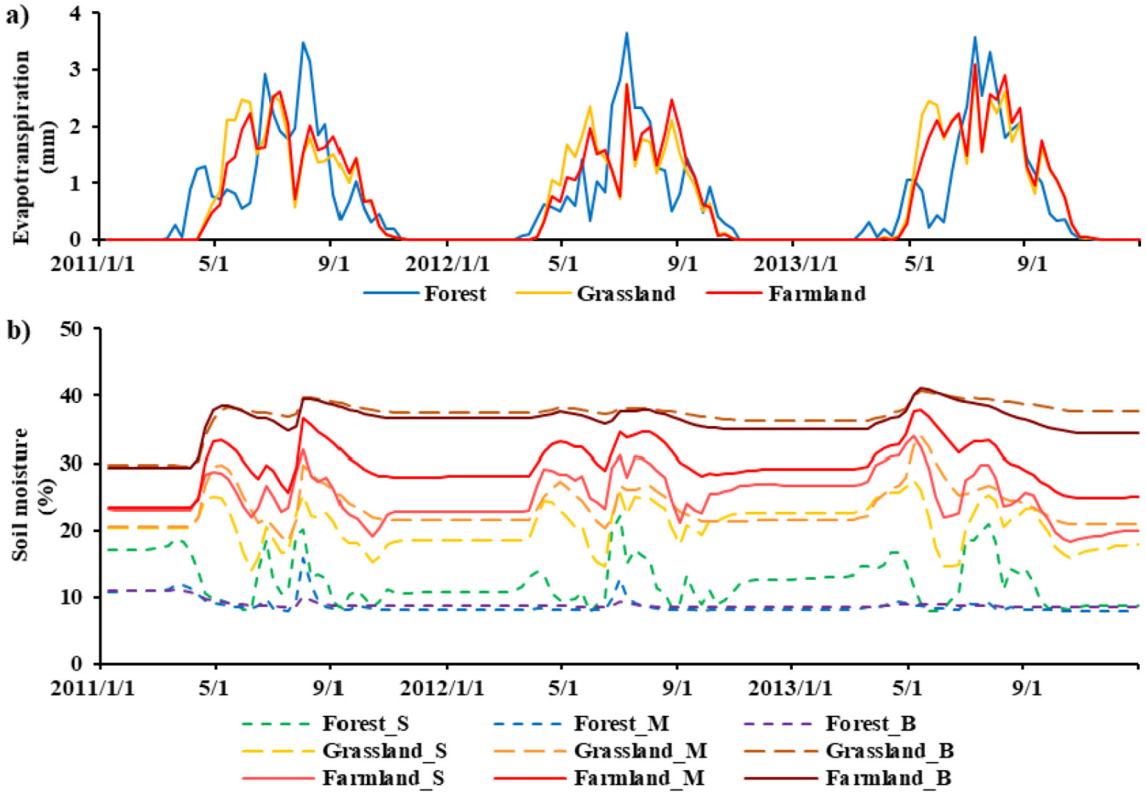

Fig. 6. Daily area-averaged a) evapotranspiration and b) soil moisture of the three layers during 2011 to 2013. S means the surface layer, M means the middle layer, B means the bottom layer.

2.2. Model description and modification

The DHSVM is a physically based, spatially explicit model that is designed to simulate hydrological processes in complex terrains. This model solves water and energy balances for each grid cell at a sub-daily time scale. The evapotranspiration is calculated by the Penman-Monteith equation. A two-layer mass energy balance model is used to calculate snow hydrological processes and changes in the snowpack heat content. Unsaturated moisture movement through the three-layer root-zone soil above the water table is derived using Darcy's law. Surface runoff and saturated subsurface flow to streams are modeled cell-by-cell using a kinematic or diffusion approximation and finally routed downstream using the linear reservoir method. A detailed description of the model can be found in Wigmosta et al. (1994) and Wigmosta et al. (2002).

To incorporate the remotely sensed LAI data, the DHSVM model was modified as follows. First, we altered the time frequency of the reading vegetation parameters of each land use type, including LAI and two intermediate variables (i.e., maximum interception storage and transmission of diffuse radiation), from 1 month to 8 days, corresponding to temporal resolution of the remotely sensed product. Second, the file path of remotely sensed LAI data was added into the configuration file, and a new function was then built to read the LAI data and write it into a structure array which can temporarily store the vegetation information for each grid cell with a time interval of 8 days.

2.3. Experimental design

Two numerical experiments (i.e., L_Class and L_Pixel) are designed to evaluate the impacts of the spatial distribution of LAI on hydrological simulations. L_Class uses 8-day remotely sensed LAI averaged for each vegetation type, while L_Pixel uses the 8-day remotely sensed LAI data for each grid cell. Both L_Class and L_Pixel updates LAI per 8 days, keeping other parameters constant.

Based on the hydrological simulation results from L_Pixel, the multiple linear stepwise regression analysis is further used to detect the impacts of meteorological factors and LAI on hydrological elements during the growing season at the pixel scale. Meteorological factors include air temperature, wind speed, relative humidity, shortwave radiation, and precipitation, while hydrological elements include evapotranspiration and soil moisture of the three layers (corresponding to the three-layer root-zone soil). In addition, water availability (precipitation minus evapotranspiration) is added as a new dependent variable for regression analysis to provide valuable information for water resource optimization management. Precipitation minus evapotranspiration determines the sum of surface and subsurface water, which has been widely used in the water cycle researches (Swenson and Wahr, 2006; Byrne and O'Gorman, 2015). All the above variables are averaged per 8 days during the growing season before regression analysis.

2.4. Model required inputs

2.4.1. Meteorological inputs

Daily meteorological data required in the model, such as air temperature (°C), wind speed (m/s), relative humidity (%), and sunshine duration (h), were obtained from the 6 meteorological stations, provided by China Meteorological Administration (CMA; http://data.cma.cn/). Daily precipitation data was recorded by 25 rain gauges, 6 of which were included in meteorological stations, while others were gathered from the Hydrological Yearbook (Hydrological Bureau et al., 2014). The precipitation data were then spatially interpolated to 250-m grid spacing via the Kriging interpolation method (Oliver and Webster, 1990).

Fig. 7. Regression coefficients between the evapotranspiration and the influential factors during the growing season. The yellow color with zero value indicates that the relationships between the evapotranspiration and the influential factors were not significant. (For interpretation of the references to color in this figure legend, the reader is referred to the web version of this article.)

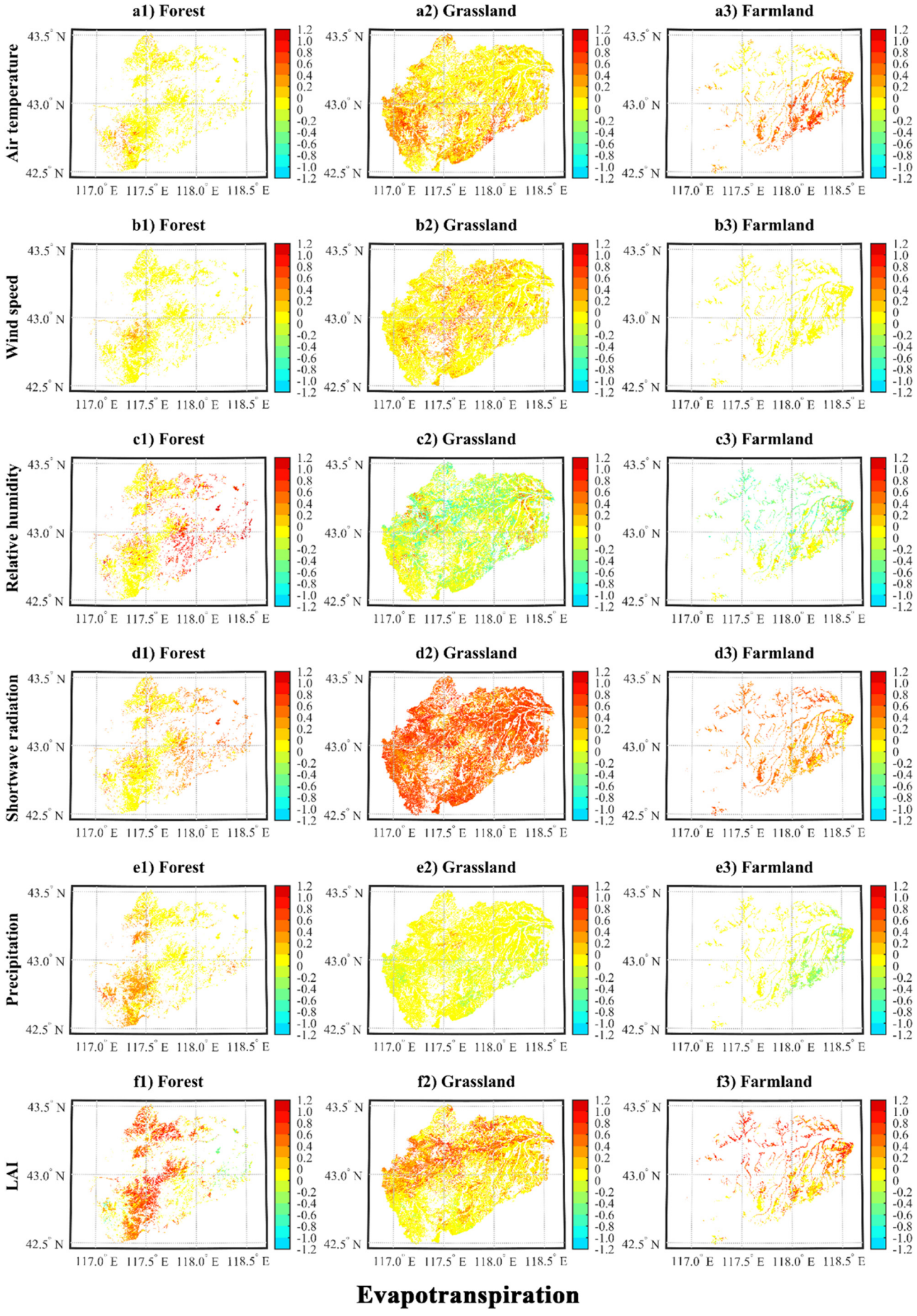
a1) Forest
a2) Grassland
a3) Farmland
b1) Forest
b2) Grassland
b3) Farmland
c1) Forest
c2) Grassland
c3) Farmland
d1) Forest
d2) Grassland
d3) Farmland
e1) Forest
e2) Grassland
e3) Farmland
f1) Forest
f2) Grassland
f3) Farmland
Air temperature
Wind speed
Relative humidity
Shortwave radiation
Precipitation
LAI
43.5° N
43.0° N
42.5° N
117.0° E
117.5° E
118.0° E
118.5° E
1.2
1.0
0.8
0.6
0.4
0.2
0
0
-0.2
-0.4
-0.6
-0.8
-1.0
-1.2
Evapotranspiration

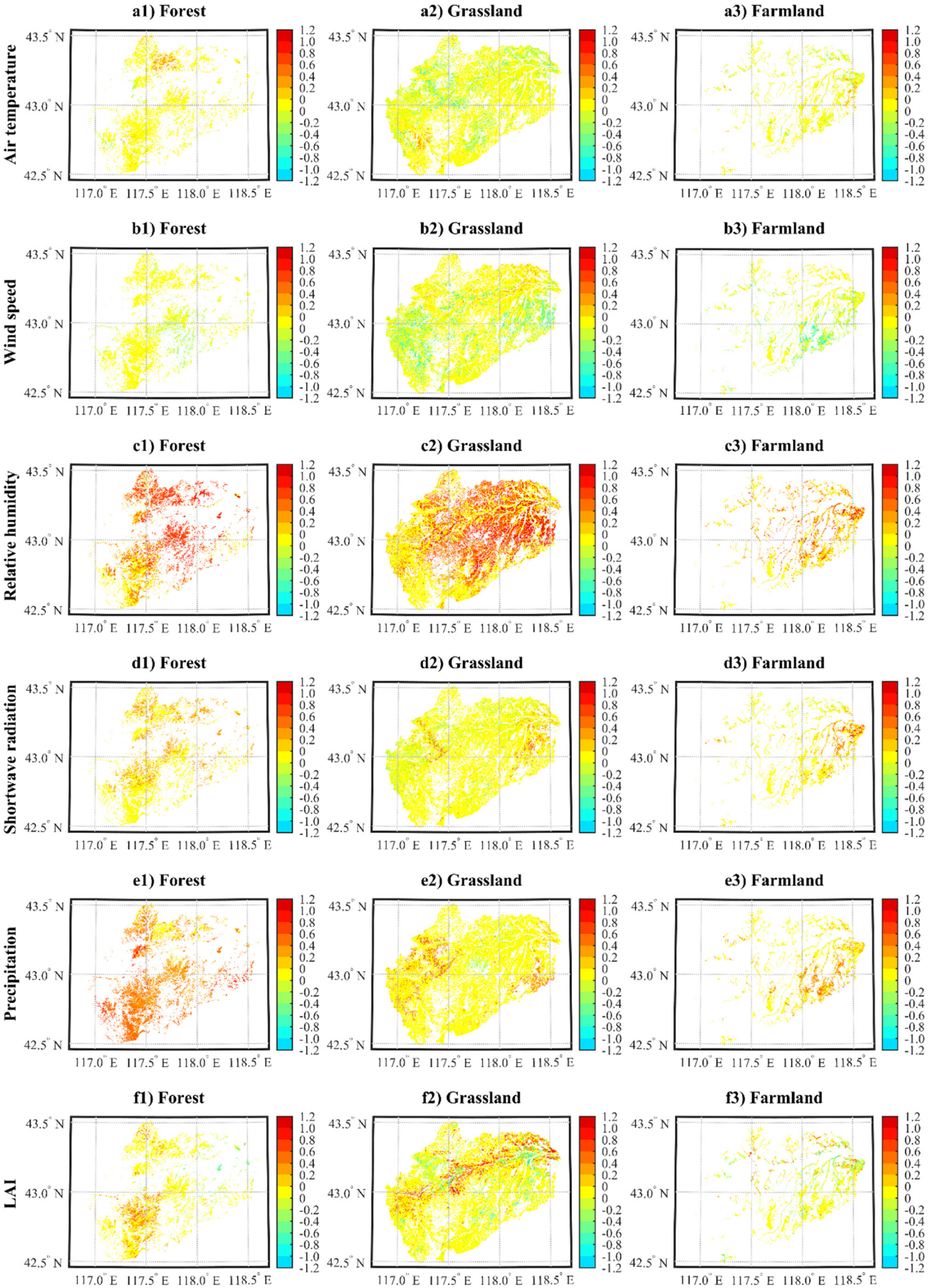
a1) Forest
a2) Grassland
a3) Farmland
b1) Forest
b2) Grassland
b3) Farmland
c1) Forest
c2) Grassland
c3) Farmland
d1) Forest
d2) Grassland
d3) Farmland
e1) Forest
e2) Grassland
e3) Farmland
f1) Forest
f2) Grassland
f3) Farmland
Air temperature
Wind speed
Relative humidity
Shortwave radiation
Precipitation
LAI
43.5° N
43.0° N
42.5° N
117.0° E
117.5° E
118.0° E
118.5° E
1.2
1.0
0.8
0.6
0.4
0.2
0
0
-0.2
-0.4
-0.6
-0.8
-1.0
-1.2
Soil moisture of the surface layer

Moreover, the incoming shortwave radiation (W/m^2) was calculated using the Angstrom–Prescott (AP) equation (Angstrom, 1924; Prescott, 1940) and it was further used to calculate the incoming longwave radiation (W/m^2) (Bohn et al., 2013).

2.4.2. Spatial inputs

In our study, the model is run with 250-m grid spacing. This 250-m resolution is reasonable because of the relatively homogenous topographical conditions within a grid cell. Elevation data was obtained from the 3 arc-seconds SRTM (Shuttle Radar Topography Mission) DEM (Farr et al., 2007), provided by International Scientific & Technical Data Mirror Site, constructed by Chinese Academy of Sciences (http://www.gscloud.cn/). The DEM was further utilized to calculate the watershed boundary and create the slope. Soil depth (Fig. 1c) and river network (Fig. 1d) were generated from the DEM using an ARC Macro Language (AML) program provided by DHSVM website (https://dhsvm.pnnl.gov/). Soil type data was obtained from the Harmonized World Soil Database v1.1 (Fischer et al., 2008), provided by Cold and Arid Regions Sciences Data Center (http://westdc.westgis.ac.cn/). Loam (29.6%), silt loam (24.1%), sand (22.5%), and sandy loam (11.6%) are the four major soil types in the study area. Land use data for 2010 with a 30-m resolution was obtained from the National Earth System Science Data Sharing Infrastructure (http://www.geodata.cn/) to represent a static land use distribution during 2011–2013 (Fig. 1a). All gridded inputs were projected into unified projection coordinate system and resampled at a spatial resolution of 250 m.

2.4.3. Model parameterization

Several vegetation parameters (e.g., minimum stomatal resistance, LAI, albedo, vegetation height, and vapor pressure deficit) and soil parameters (e.g., lateral saturated hydraulic conductivity, exponential decrease rate of conductivity, porosity, field capacity, and wilting point) have been demonstrated to be highly sensitive to streamflow in the DHSVM model (Lan et al., 2011b; Du et al., 2014). For model parameterization, LAI was obtained from the global land surface satellite product (GLASS; http://www.geodata.cn/), with a spatial resolution of 1 km for the 46 retrieval periods per year (i.e., 1, 9, …, 361). Meanwhile, the forest LAI was divided into overstory (70% of total LAI) and understory LAI (30% of total LAI) (Chianucci et al., 2016; Liu et al., 2017). The 8-day area-average albedos for each land use type as a vegetation parameter inputs were derived from a 30-arc, 8-day global gap-filled, snow-free albedo data archive (ftp://rsftp.eeos.umb.edu/). A temporal interpolation technique (Gao et al., 2008) was applied to the spatially complete albedo data set to fill the MODIS albedo product for which there were no observations, were of low quality, or were snow covered with geophysical realistic values (Sun et al., 2017). Porosity, field capacity, wilting point and lateral saturated hydraulic conductivity were calculated using the Soil Plant Atmosphere Water (SPAW) model (Saxton, 1989). Exponential decrease rate of conductivity, vapor pressure deficit, vegetation height, and minimum stomatal resistance were adjusted as described by Lan et al. (2011b). All soil and vegetation parameters and their sources are presented in Tables 1 and 2.

2.5. Model calibration and validation

Daily observed streamflow of the Balin Bridge hydrological station from 2011 to 2013 were gathered from the Hydrological Yearbook for model calibration and validation. The model was calibrated from January 1, 2011 to December 31, 2011 and validated from January 1, 2012 to December 31, 2013. We employed four statistical criteria to evaluate streamflow prediction, including Nash-Sutcliffe Efficiency (NSE; Nash and Sutcliffe, 1970), coefficient of determination (R^2), root mean squared error (RMSE), and percent bias (PBIAS; Moriasi et al., 2007).

In addition, daily mean remotely sensed evapotranspiration during the growing season with 500-m resolution, derived from the MOD16 global evapotranspiration product (http://modis.gsfc.nasa.gov/), was used as spatial reference to verify the simulation results. MOD16 product has been assessed in various watersheds of China and shows rational simulation accuracy in the Liaohe River basin (He and Shao, 2014; Du and Song, 2018). First, we resampled daily mean simulated evapotranspiration during the growing season to 500-m resolution. Then, *Z*-score standardization was performed for the remotely sensed and simulated evapotranspiration. Finally, we calculated the Kendall's tau correlation coefficients between the remotely sensed and simulated evapotranspiration to compare their spatial congruence. While remotely sensed output for soil moisture was not used to compare with our simulations due to its coarse resolution and the uncertainty of the retrieval algorithm (Goward et al., 2002; Wan et al., 2005; Yan, 2007).

3. Results and discussions

3.1. Model evaluation

The observed and simulated daily streamflow during the growing season from 2011 to 2013 are presented in Fig. 3. It's found that the spatial distribution of LAI doesn't result in a significant change in variability of streamflow, but the magnitude of streamflow in L_Pixel has a 20.35% increase than that in L_Class during the growing season. Meanwhile, compared to the average streamflow of L_Class (i.e., 10.01 m^3/s), that of L_Pixel (i.e., 12.04 m^3/s) is closer to the observed values (i.e., 12.35 m^3/s). The change in runoff is driven mainly by the change in precipitation (Zheng et al., 2018). Landscape pattern changes mainly affect the magnitude of streamflow instead of its variation trend, which is consistent with the scenario analysis results of Chu et al. (2010) and Lan et al. (2011a). In addition, four evaluation indicators in Table 3 indicate that streamflow of L_Pixel is more accurate than that of L_Class. Although this improvement is slight, it's meaningful for streamflow simulation in basins where the range of LAI is much larger.

Simulation results of evapotranspiration are significantly different in L_Pixel and L_Class. Kendall's tau correlation coefficients between the L_Class (Fig. 4a) and L_Pixel (Fig. 4b) and MODIS-based evapotranspiration (Fig. 4d) are 0.192 ($p < 0.01$) and 0.437 ($p < 0.01$), respectively, indicate that accurately representing the spatial heterogeneity of LAI can improve the spatial distribution simulation of evapotranspiration. Both the interception and transpiration, as the two of the most important components of the evapotranspiration, are primarily determined by LAI (van der Ent et al., 2014), which explains the similarity between the spatial distribution of evapotranspiration relative difference (Fig. 4c) and LAI (Fig. 2f).

Soil water is not only affected by meteorological factors and land use pattern, but also by soil depth and topographical factor, such as elevation, slope, and aspect (He et al., 2003). In our study, the spatial distribution of simulated three-layer root-zone soil moisture (Fig. S2) is similar to that of soil depth (Fig. 1c). Thicker soil depth corresponds to higher soil moisture. Thus, LAI has less influence on the spatial distribution of soil moisture than soil depth. In addition, the relative difference (L_Pixel minus L_Class divided by L_Class) of simulated soil moistures during the growing season decreases with the deepening of soil layer (Fig. 5), which means that surface soil water is more sensitive to the spatial heterogeneity of LAI. Although there is no site data of soil moisture in our study area to identify the model performance, it's meaningful to incorporate more physically realistic LAI into the model, which can

Fig. 8. Regression coefficients between the soil moisture of the surface layer and the influential factors during the growing season. The yellow color with zero value indicates that the relationships between the soil moisture of the surface layer and the influential factors were not significant. (For interpretation of the references to color in this figure legend, the reader is referred to the web version of this article.)

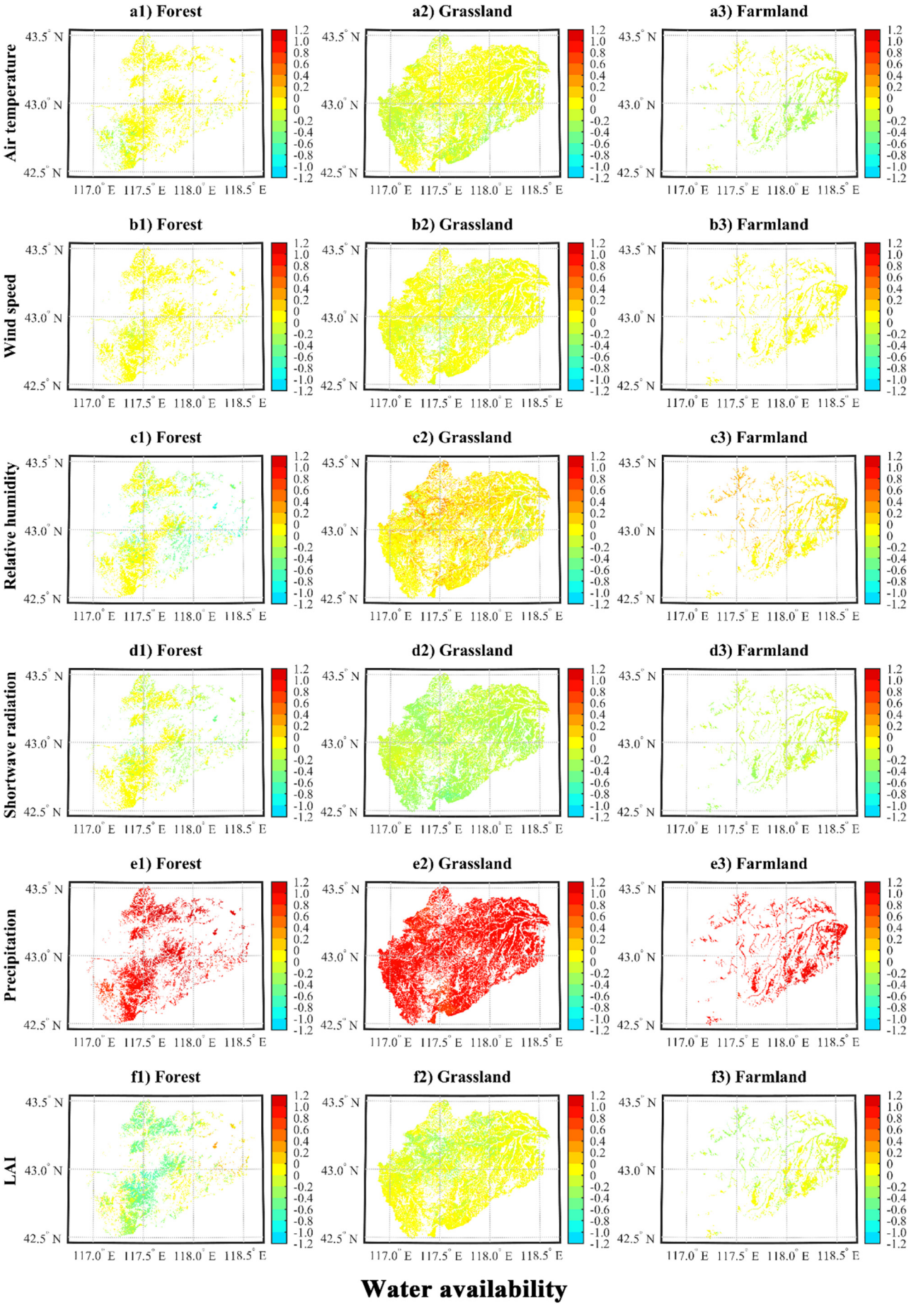
a1) Forest
a2) Grassland
a3) Farmland
b1) Forest
b2) Grassland
b3) Farmland
c1) Forest
c2) Grassland
c3) Farmland
d1) Forest
d2) Grassland
d3) Farmland
e1) Forest
e2) Grassland
e3) Farmland
f1) Forest
f2) Grassland
f3) Farmland
Air temperature
Wind speed
Relative humidity
Shortwave radiation
Precipitation
LAI
43.5° N
43.0° N
42.5° N
117.0° E 117.5° E 118.0° E 118.5° E
1.2 1.0 0.8 0.6 0.4 0.2 0 0 -0.2 -0.4 -0.6 -0.8 -1.0 -1.2
Water availability

promote the performance of soil moisture simulations to land use management, especially in the semi-arid regions.

3.2. Hydrological dynamic characteristics in different land use types

Based on the simulation results of L_Pixel, dynamic changes of evapotranspiration and soil moisture of the three land use types during 2011–2013 are presented in Fig. 6. Evapotranspiration of the forest, grassland, and farmland are mainly distributed in the growing season (Fig. 6a). Evapotranspiration and soil moisture have obvious seasonal variations. In the arid and semi-arid regions, evapotranspiration is positively affected by soil moisture (Zuo et al., 2011; Wang et al., 2016). There are significant differences in soil moisture among different land use types. The order of soil moisture is farmland > grassland > forest (Fig. 6b), which is consistent with the field measurement of Gong et al. (2004) in semi-arid areas. This is because that forests have greater LAI and richer roots that consumes more water through interception and transpiration. It's worth noting that the surface soil moisture is largest among the three soil layers of the forest, but it is at a minimum among those of the grassland and farmland (Fig. 6b). This finding is observed because the root system of the forest is mainly distributed in the bottom two layers, while that of the grassland and farmland is opposite.

3.3. Influential factors of the hydrological elements during the growing season

3.3.1. Influential factors of evapotranspiration

Regression coefficients between the evapotranspiration and the six influential factors during the growing season for the three land use types are presented in Fig. 7. LAI is the most important factor positively affecting forest evapotranspiration (Fig. 7f1). LAI can promote vegetation interception and transpiration (Monteith, 1965) and affects evapotranspiration of grasslands and farmlands in the same way (Fig. 7 f2, f3). In the grassland and farmland, shortwave radiation is the most important factor (Fig. 7 d2, d3) that enhances evapotranspiration by directly increasing land surface net radiation.

In addition, the increase in air temperature not only positively affects potential evaporation rate, but also reduce canopy resistance within a certain temperature range (Dickinson et al., 1993), thus leading to the increase of both evaporation and transpiration in grasslands and farmlands (Fig. 7a2, a3). Aerodynamic resistance is inversely associated with wind speed (Storck, 2000) and has a negative influence on potential evaporation rate (Wigmosta et al., 1994). So, wind speed has a positive effect on grassland evapotranspiration (Fig. 7b2). Precipitation promotes forest evapotranspiration by increasing interception and soil moisture (Fig. 7e1).

Relative humidity is the ratio of the actual water vapor pressure to the saturation vapor pressure, which has different effects on evapotranspiration in different land use types (Fig. 7c1, c2, c3). At a certain air temperature, the increase in relative humidity decreases vapor pressure deficit (saturation vapor pressure minus actual water vapor pressure). The decrease of vapor pressure deficit can directly decrease potential evaporation rate and further decrease transpiration rate (Wigmosta et al., 1994). However, it can also promote transpiration rate by reducing canopy resistance (Dickinson et al., 1993). As evapotranspiration of grasslands and farmlands is negatively affected by relative humidity (Fig. 7c2, c3), it's rational that evaporation dynamic dominates the evapotranspiration change. In the forest, limited soil water restricts its transpiration and evaporation. While relative humidity is positively related to surface soil moisture in the semi-arid regions (Ravi et al., 2004), which results in the increase of forest evapotranspiration (Fig. 7c1).

3.3.2. Influential factors of soil moisture

Regression coefficients between the soil moisture of the surface layer and the influential factors during the growing season for the three land use types are presented in Fig. 8. Relative humidity is the most important factors in the forest, grassland, and farmland (Fig. 8c1, c2, c3), which promotes surface soil moisture by decreasing vegetation transpiration and surface soil evaporation. In addition, the increase in precipitation directly increases forest soil water (Fig. 8e1). While the increase in air temperature promotes potential evaporation rate and thus grassland transpiration, leading to the decrease of surface soil moisture in the grassland (Fig. 8a2). Wind speed negatively affects soil moisture in the grassland and farmland by increasing evapotranspiration (Fig. 8b2, b3). Moreover, the increase of LAI decreases the shortwave radiation transmitted from the canopy (Monteith, 1965), further increasing the net radiation absorbed by the canopy. Thus, the undergrowth vegetation obtained less energy, leading to the decrease in the evaporation of the surface soil water and the increase in surface soil moisture of forests (Fig. 8f1). Similarly, the increase in the grassland LAI increased the surface soil moisture (Fig. 8f2). The effects of these factors on soil moisture significantly decreases with the deepening of soil layer (Figs. S3 and S4).

3.3.3. Influential factors of water availability

Regression coefficients between the water availability and the influential factors during the growing season for the three land use types are presented in Fig. 9. Obviously, precipitation is the most important influential factor positively correlated with water availability in forests, grasslands, and farmlands (Fig. 9 e1, e2, e3). Apart from precipitation, LAI is the key factor negatively affecting water availability of the forest (Fig. 9f1), while shortwave radiation is the key factor negatively affecting that of the grassland and farmland (Fig. 9 d2, d3). What's more, relative humidity has slight but different effects on water availability in a slight part of forests and grasslands (Fig. 9 c1, c2), which is opposite to its effect on evapotranspiration (Fig. 7 c1, c2). Air temperature is negatively affecting water availability of grassland and farmland (Fig. 9 a2, a3) by promoting evapotranspiration.

3.4. Implications for water resource optimization management

Our study provides valuable information for water resource optimization management in terms of promoting adaptation to climate change and human water requirement via land use pattern management. In the past 65 years, the mean air temperature showed a wavelike rising trend in the Xar Moron River basin, and at the same time, precipitation showed a decreasing trend, especially during the summer (Yao et al., 2016). Compared with grasslands and farmlands, precipitation significantly promotes evapotranspiration in forests, which means that forests trend to consume more water for growth in this basin. Afforestation is the better option for the semi-arid regions only in areas where the annual precipitation is >500 mm, and at this time, afforestation will not induce the soil desiccation (Ren et al., 2018). Otherwise, afforestation promotes both evapotranspiration and soil moisture, greatly decreasing water availability and streamflow in this semi-arid basin.

Hydrological elements of grasslands are more sensitivity to air temperature than these of forests. The increase in grassland air temperature enhances the evapotranspiration and reduces water availability. Forest seems to be more resilient to the warming activity, but in fact forest keeps least soil water which limits its evapotranspiration.

Therefore, to mitigate the negative effects of drying and warming climate on watershed water availability, the landscape managers can decrease forest area to decrease the total evapotranspiration and to further

Fig. 9. Regression coefficients between the water availability and the influential factors during the growing season. The yellow color with zero value indicates that the relationships between the water availability and the influential factors were not significant. (For interpretation of the references to color in this figure legend, the reader is referred to the web version of this article.)

increase water availability in this semi-arid basin. Moreover, vegetation management measures (e.g., tree surgery and return forest to grassland) can be used to increase water availability by decreasing the forest LAI and increase the grassland LAI.

4. Conclusions

Our study analyzed the hydrological elements and associated influential factors for different land use types in a semi-arid basin during the growing season from 2011 to 2013 by incorporating high-resolution remotely sensed LAI into a modified distributed hydrological model. The results confirm that integrating the spatial heterogeneity of the LAI has slight improvement on streamflow simulations and significantly promotes the model performance of spatial hydrological element simulations. Hydrological elements vary in the different land use types. Especially, the soil moisture of forests is significantly lower than that of grasslands and farmlands. In the study area, hydrological elements are driven by various influential factors, among which precipitation, LAI, and relative humidity are the three most critical influential factors in the forest, while hydrological elements in the grassland and farmland are mainly affected by shortwave radiation, relative humidity, air temperature, and LAI. LAI has positive effects on evapotranspiration and soil moisture and further reduced the water availability and runoff. Compared with grasslands and farmlands, LAI has greater negative influence on forest water availability. At the same time, the increase in precipitation has greater positive effects on evapotranspiration and soil moisture of forests than these of grasslands and farmlands. Therefore, to mitigate the negative effects of drying and warming climate, increase water availability, and satisfy increasing human water demand, the forest area should be converted into grassland while the native grassland should be maintained for soil water conservation. Landscape planning and management are helpful in promoting the regional sustainable utilization of water resources.

Acknowledgments

This study was supported by the Programs of the National Natural Science Foundation of China (41571170), the Fund for Creative Research Groups of the National Natural Science Foundation of China (41621061), the Project of the State Key Laboratory of Earth Surface Processes and Resource Ecology, the National Natural Science Foundation of China (41801179), the Beijing Normal University Interdisciplinary Research Foundation for the First-Year Doctoral Candidates (BNUXKJC1809), and the China Postdoctoral Science Foundation (2017M620664).

Appendix A. Supplementary data

Supplementary data to this article can be found online at https://doi.org/10.1016/j.scitotenv.2019.07.068.

References

Alvarenga, L.A., De Mello, C.R., Colombo, A., Cuartas, L.A., Bowling, L.C., 2016. Assessment of land cover change on the hydrology of a Brazilian headwater watershed using the Distributed Hydrology-Soil-Vegetation Model. Catena 143, 7–17.
Angstrom, A., 1924. Solar and terrestrial radiation. Q. J. Roy. Meteor. Soc. 50 (210), 121–126.
Arnold, J.G., Fohrer, N., 2005. Swat 2000: current capabilities and research opportunities in applied watershed modelling. Hydrol. Process. 19 (3), 563–572.
Bohn, T.J., Livneh, B., Oyler, J.W., Running, S.W., Nijssen, B., Lettenmaier, D.P., 2013. Global evaluation of mtclim and related algorithms for forcing of ecological and hydrological models. Agric. For. Meteorol. 176 (13), 38–49.
Breuer, L., Eckhardt, K., Frede, H.G., 2003. Plant parameter values for models in temperate climates. Ecol. Model. 169 (2–3), 237–293.
Byrne, M.P., O'Gorman, P.A., 2015. The response of precipitation minus evapotranspiration to climate warming: why the "wet-get-wetter, dry-get-drier" scaling does not hold over land. J. Clim. 28 (20), 8078–8092.
Campbell, G.S., Norman, J.M., 1979. An introduction to environmental biophysics/G. S. Campbell. J. M. Norman. Biol. Plantarum 21 (2), 104.
Cao, Q., Yu, D., Georgescu, M., Han, Z., Wu, J., 2015. Impacts of land use and land cover change on regional climate: a case study in the agro-pastoral transitional zone of China. Environ. Res. Lett. 10 (12), 124025.
Chen, J.M., Rich, P.M., Gower, S.T., Norman, J.M., Plummer, S., 1997. Leaf area index of boreal forests: theory, techniques, and measurements. J. Geophys. Res. 102, 29429–29443.
Chianucci, F., Minari, E., Fardusi, M.J., Merlini, P., Cutini, A., Corona, P., Mason, F., 2016. Relationships between overstory and understory structure and diversity in semi-natural mixed floodplain forests at bosco Fontana (Italy). IForest 9 (6).
Chu, H.J., Lin, Y.P., Huang, C.W., Hsu, C.Y., Chen, H.Y., 2010. Modelling the hydrologic effects of dynamic land-use change using a distributed hydrologic model and a spatial land-use allocation model. Hydrol. Process. 24 (18), 2538–2554.
van Dam, J.C. (Ed.), 2003. Impacts of Climate Change and Climate Variability on Hydrological Regimes. Cambridge University Press, Cambridge.
Dickinson, R.E., Henderson-Sellers, A., Kennedy, P.J., 1993. Biosphere-Atmosphere Transfer Scheme (BATS) Version 1e as Coupled to the NCAR Community Climate Model, NCAR Technical Note, NCARITN-387+STR, Boulder, Colorado.
Donohue, R.J., Roderick, M.L., Mcvicar, T.R., 2007. On the importance of including vegetation dynamics in budyko's hydrological model. Hydrol. Earth Syst. Sci. 3 (4), 983–995.
Du, J., Song, K., 2018. Validation of global evapotranspiration product (MOD16) using flux tower data from Panjin coastal wetland, Northeast China. Chin. Geogr. Sci. 28 (3), 420–429.
Du, E., Link, T.E., Gravelle, J.A., Hubbart, J.A., 2014. Validation and sensitivity test of the distributed hydrology soil-vegetation model (DHSVM) in a forested mountain watershed. Hydrol. Process. 28 (26), 6196–6210.
Eagleson, P.S., 2005. Ecohydrology: Darwinian Expression of Vegetation Form and Function. Cambridge University Press, Cambridge.
van der Ent, R.J., Wang-Erlandsson, L., Keys, P.W., Savenije, H.H.G., 2014. Contrasting roles of interception and transpiration in the hydrological cycle - part 2: moisture recycling. Earth Syst. Dynam. 5, 471–489.
Farr, T.G., Rosen, P.A., Caro, E., Crippen, R., Duren, R., Hensley, S., et al., 2007. The shuttle radar topography mission. Rev. Geophys. 45, RG2004.
Fischer, G., Nachtergaele, F., Prieler, S., van Velthuizen, H. T., Verelst, L., Wiberg, D., 2008. Global Agro-ecological Zones Assessment for Agriculture (GAEZ 2008). IIASA, Laxenburg, Austria and FAO, Rome, Italy.
Ford, T.W., Quiring, S.M., 2013. Influence of MODIS-derived dynamic vegetation on VIC-simulated soil moisture in Oklahoma. J. Hydrometeorol. 14 (6), 1910–1921.
Fu, B., Zhao, W., Chen, L., Liu, Z., Lü, Y., 2005. Eco-hydrological effects of landscape pattern change. Landsc. Ecol. Eng. 1 (1), 25–32.
Fujimoto, M., Ohte, N., Tani, M., 2008. Effects of hillslope topography on hydrological responses in a weathered granite mountain, Japan: comparison of the runoff response between the valley-head and the side slope. Hydro. Process. 22 (14), 2581–2594.
Gao, F., Morisette, J.T., Wolfe, R.E., Ederer, G., Pedelty, J., Masuoka, E., Myneni, R., Tan, B., Nightingale, J., 2008. An algorithm to produce temporally and spatially continuous MODIS-LAI time series. IEEE Geosci. Remote Sens. Lett. 5 (1), 60–64.
Gao, H., Sabo, J.L., Chen, X., Liu, Z., Yang, Z., Ren, Z., et al., 2018. Landscape heterogeneity and hydrological processes: a review of landscape-based hydrological models. Landsc. Ecol. 1–20.
Gong, J., Chen, L., Fu, B., Chen, X., Huang, Y., Huang, Z., 2004. Study on soil moisture effect of vegetation restoration in small watershed of loess hilly region. Paper Presented at National Congress of the Chinese Ecological Society, Sichuan.
Goudriaan, J., 1977. Crop Micrometeorology: A Simulation Study. Centre for Agricultural Publishing and Documentation, Wageningen.
Goward, S.N., Xue, Y., Czajkowski, K.P., 2002. Evaluating land surface moisture conditions from remotely sensed/vegetation index measurements—an exploration with the simplified simple biosphere model. Remote Sens. Environ. 79, 225–242.
Haddeland, I., Skaugen, T., Lettenmaier, D.P., 2006. Anthropogenic impacts on continental surface water fluxes. Geophys. Res. Lett. 33, L08406.
He, T., Shao, Q., 2014. Spatial-temporal variation of terrestrial evapotranspiration in China from 2001 to 2010 using MOD16 products. J. Geogr. Inf. Sci. 16 (6), 979–988.
He, Q.H., He, Y.H., Bao, W.K., 2003. Research on dynamics of soil moisture in arid and semiarid mountainous areas. J. Mt. Sci-Engl. 21 (2), 149–156.
Huxman, T.E., Wilcox, B.P., Breshears, D.D., Scott, R.L., Snyder, K.A., Small, E.E., et al., 2005. Ecohydrological implications of woody plant encroachment. Ecology 86, 308–319.
Hydrological Bureau, Chinese State Ministry of Water Resources, 2012, 2013, 2014. Annual Hydrological Report, P. R. China, Hydrological Data of Liaohe River Basin, Upstream Basin of Liaohe River (Upstream of Zhengjiatun) (2011, 2012, 2013). China Water & Power Press: Beijing, China, vol. 2, No.1. (in Chinese and issued for internal use).
Jiao, Y., Lei, H., Yang, D., Huang, M., Liu, D., Yuan, X., 2017. Impact of vegetation dynamics on hydrological processes in a semi-arid basin by using a land surface-hydrology coupled model. J. Hydrol. 551, 116–131.
Lan, C., Beyene, T.K., Voisin, N., Su, F., Lettenmaier, D.P., Alberti, M., Richey, J.E., 2011a. Effects of mid-twenty-first century climate and land cover change on the hydrology of the puget sound basin, Washington. Hydrol. Process. 25 (11), 1729–1753.
Lan, C., Giambelluca, T.W., Ziegler, A.D., 2011b. Lumped parameter sensitivity analysis of a distributed hydrological model within tropical and temperate catchments. Hydrol. Process. 25 (15), 2405–2421.
Liu, W., Xu, Z., Li, F., Zhang, L., Zhao, J., Yang, H., 2015. Impacts of climate change on hydrological processes in the Tibetan plateau: a case study in the Lhasa river basin. Stoch. Env. Res. Risk A. 29 (7), 1809–1822.
Liu, Y., Liu, R., Pisek, J., Chen, J.M., 2017. Separating overstory and understory leaf area indices for global needleleaf and deciduous broadleaf forests by fusion of modis and misr data. Biogeosciences 14 (5), 1–32.
Ma, F., Li, X., Zhang, J., Li, A., 2006. Spatial heterogeneity of soil moisture in Shapotou sand-fixing artificial vegetation area. Chin. J. Appl. Ecol. 17 (5), 789–795.

Ma, Q., Zavattero, E., Du, M., Vo, N.D., Gourbesville, P., 2016. Assessment of high-resolution topography impacts on deterministic distributed hydrological model in extreme rainfall-runoff simulation. Procedia. Eng. 154, 601–608.
Meyer, P.D., Rockhold, M.L., Gee, G.W., 1997. Uncertainty Analyses of Infiltration and Subsurface Flow and Transport for SDMP Sites (No. NUREG/CR–6565; PNNL–11705). Nuclear Regulatory Commission, Div. Of Regulatory Applications, Washington; Pacific Northwest National Laboratory, Richland.
Monteith, J.L., 1965. Evaporation and Environment. 19th Symposia of the Society for Experimental Biology. vol. 19. university Press, Cambridge, pp. 205–234.
Moriasi, D.N., Arnold, J., VanLiew, M.W., Bingner, R.L., Harmel, R.D., Veith, T.L., 2007. Model evaluation guidelines for systematic quantification of accuracy in watershed simulations. T. Am. Soc. Agr. Biol. Eng. 50, 885–900.
Nash, J.E., Sutcliffe, J.V., 1970. River flow forecasting through conceptual models. Part I—A discussion of principles. J. Hydrol. 10 (3), 282–290.
Nijssen, B., Lettenmaier, D.P., 1999. A simplified approach for predicting shortwave radiation transfer through boreal forest canopies. J. Geophys. Res.-Atmos. 104 (D22), 27859–27868.
Oliver, M.A., Webster, R., 1990. Kriging: a method of interpolation for geographical information systems. Int. J. Geogr. Inf. Syst. 4 (3), 313–332.
Parr, D., Wang, G., Bjerklie, D., 2015. Integrating remote sensed data on evapotranspiration and leaf area index with hydrological modeling: impacts on model performance and future predictions. J. Hydrometeorol. 16 (5), 150602141504006.
Prescott, J.A., 1940. Evaporation from a water surface in relation to solar radiation. Trans. R. Soc. S. Aust. 64, 114–118.
Ravi, S., D'Odorico, P., Over, T.M., Zobeck, T.M., 2004. On the effect of air humidity on soil susceptibility to wind erosion: the case of air-dry soils. Geophys. Res. Lett. 31 (L09501), 1–4.
Ren, Z., Li, Z., Liu, X., Li, P., Cheng, S., Xu, G., 2018. Comparing watershed afforestation and natural revegetation impacts on soil moisture in the semiarid loess plateau of China. Sci. Rep. 8 (1), 2972.
Saxton, K.E., 1989. User's Manual for SPAW: A Soil-Plant-Atmosphere-Water Model. USDAARS, Pullman, Washington.
Schnorbus, M., Werner, A., Bennett, K., 2014. Impacts of climate change in three hydrologic regimes in British Columbia, Canada. Hydrol. Process. 28 (3), 1170–1189.
Sellers, P.J., Tucker, C.J., Collatz, G.J., Los, S.O., Justice, C.O., Dazlich, D.A., et al., 1994. A global 1° by 1° NDVI data set for climate studies. Part 2: the generation of global fields of terrestrial biophysical parameters from the NDVI. Int. J. Remote Sens. 15 (17), 3519–3545.
Skamarock, W.C., Klemp, J.B., 2008. A time-split nonhydrostatic atmospheric model for weather research and forecasting applications. J. Comput. Phys. 227, 3465–3485.
Stagl, J., Mayr, E., Koch, H., Hattermann, F.F., Huang, S., 2014. Effects of climate change on the hydrological cycle in central and Eastern Europe. In: Rannow, S., Neubert, M. (Eds.), Managing Protected Areas in Central and Eastern Europe Under Climate Change. Springer Netherlands, Berlin, pp. 31–43.
Stieglitz, M., Rind, D., Famiglietti, J., Rosenzweig, C., 1997. An efficient approach to modeling the topographic control of surface hydrology for regional and global climate modeling. J. Clim. 10 (1), 118–137.
Storck, P., 2000. Trees, snow and flooding: an investigation of forest canopy effects on snow accumulation and melt at the plot and watershed scales in the Pacific Northwest. Water Resour. Res., Technical Report. Dept. of Civil Engineering, University of Washington, Washington, p. 161.
Sun, G., Alstad, K., Chen, J., Chen, S., Ford, C.R., Lin, G., et al., 2011. A general predictive model for estimating monthly ecosystem evapotranspiration. Ecohydrology 4 (2), 245–255.
Sun, Q., Wang, Z., Li, Z., Erb, A., Schaaf, C.B., 2017. Evaluation of the global MODIS 30 arc-second spatially and temporally complete snow-free land surface albedo and reflectance anisotropy dataset. Int. J. Appl. Earth Obs. 58, 36–49.
Swenson, S., Wahr, J., 2006. Estimating large-scale precipitation minus evapotranspiration from grace satellite gravity measurements. J. Hydrometeorol. 7 (2), 252–269.
Thanapakpawin, P., Richey, J., Thomas, D., Rodda, S., Campbell, B., Logsdon, M., 2007. Effects of land use change on the hydrologic regime of the Mae Chaem river basin, NW Thailand. J. Hydrol. 334 (1–2), 215–230.
Vanshaar, J.R., Haddeland, I., Lettenmaier, D.P., 2002. Effects of land-cover changes on the hydrological response of interior Columbia river basin forested catchments. Hydrol. Process. 16 (13), 2499–2520.
Wan, Z., Wang, P., Li, X., 2005. Using MODIS land surface temperature and normalized difference vegetation index inputs for monitoring drought in the southern Great Plains, USA. Int. J. Remote Sens. 25 (1), 61–72.
Wang, K., Jing, X., Guo, R., Wei, S., Liang, H., 2016. Soil moisture retrieval from remote sensing and its impact on evapotranspiration in Qaidam basin. Geoscience 30 (4), 834–841.
Wigmosta, M.S., Vail, L.W., Lettenmaier, D.P., 1994. A distributed hydrology-vegetation model for complex terrain. Water Resour. Res. 30 (6), 1665–1679.
Wigmosta, M.S., Nijssen, B., Storck, P., Singh, V.P., Frevert, D.K., 2002. The distributed hydrology soil vegetation model. Mathematical Models of Small Watershed Hydrology & Applications. vol. 22(21), pp. 4205–4213.
Wu, J., An, N., Ji, Y., Wei, X., 2014. Analysis on characteristics of precipitation and runoff in Silas Mulun river basin. Meteorol. J. Inner Mongolia 4, 23–25.
Xu, X., Li, J., Tolson, B.A., 2014. Progress in integrating remote sensing data and hydrologic modeling. Prog. Phys. Geogr. 38 (4), 464–498.
Xu, L., Pyles, R.D., Paw, U., T, K., Snyder, R., Monier, E., Falk, M., et al., 2017. Impact of canopy representations on regional modeling of evapotranspiration using the WRF-ACASA coupled model. Agric. For. Meteorol. 247, 79–92.
Yan, F., 2007. Research on Model and Application of Winter Wheat Drought Monitoring from Remote Sensing Data in Hebei Province. Ph.D. Dissertation. Nanjing University.
Yang, Y., Donohue, R.J., Mcvicar, T.R., 2016. Global estimation of effective plant rooting depth: implications for hydrological modeling. Water Resour. Res. 52, 8260–8276.
Yao, S.Z., Wang, L.X., Zong, Z.H., 2016. Relationship between groundwater level and climate change in Hexigten Banner. Mod. Agric. 5, 80–81.
Zhang, Y., Wegehenkel, M., 2006. Integration of MODIS data into a simple model for the spatial distributed simulation of soil water content and evapotranspiration. Remote Sens. Environ. 104 (4), 393–408.
Zhang, G., Tao, J., Dong, J., Xu, X., 2011. Spatiotemporal variations in thermal growing seasons due to climate change in eastern Inner Mongolia during the period 1960-2010. Resour. Sci. 33 (12), 2323–2332.
Zhang, L., Nan, Z., Xu, Y., Li, S., 2016. Hydrological impacts of land use change and climate variability in the headwater region of the Heihe River basin, Northwest China. PLoS One 11 (6), e0158394.
Zheng, H., Chiew, F.H., Charles, S., Podger, G., 2018. Future climate and runoff projections across South Asia from CMIP5 global climate models and hydrological modelling. J. Hydro.: Reg. Stud. 18, 92–109.
Zhong, R., He, Y., Chen, X., 2018. Responses of the hydrological regime to variations in meteorological factors under climate change of the Tibetan plateau. Atmos. Res. 214, 296–310.
Zuo, Y., Chen, Q., Deng, Q., Tang, J., Luo, H., Wu, T., Yang, Z., 2011. Effects of soil moisture, light, and air humidity on stomatal conductance of cassava (Manihot esculenta Crantz). Chin. J. Eco. 30 (4), 689–693.